Progress In Electromagnetics Research M, Vol. 59, 9–24, 2017

An Investigation on End-Fire Radiation from Linearly Polarized Microstrip Antenna for Airborne Systems

Debajit De* and Prasanna K. Sahu

Abstract—In airborne systems, where low aerodynamic drag is urgently required, an end-fire antenna is suitable to be used. An effort to develop such an antenna, using planar elements, is described in this paper. Here, a new kind of Microstrip Slotted Antenna with end-fire properties is presented. For investigating the end-fire radiation from microstrip antenna, three antenna elements are proposed during the study — 1) Single Patch Single Feed Microstrip Slotted Antenna, 2) Dual Patch Single Feed Microstrip Slotted Antenna and 3) Dual Patch Dual Feed Microstrip Slotted Antenna. All these proposed antennas are designed and simulated in two different EM tools, which are — CST Microwave Studio (MWS) based on time domain solver and ANSYS HFSS based on frequency domain solver. Thereafter, these antenna prototype models have been fabricated and tested. Good agreement is obtained between the simulated and measured results.

1. INTRODUCTION

According to radiation characteristics, antennas are classified into two types. One is broadside antennas, and the other is end-fire antennas. A broadside antenna always radiates in perpendicular direction with respect to the plane of the antenna. In this category, some well-known topologies are monopole antenna [1], half-wavelength slotted antenna [2], and patch antenna [3]. An end-fire planar antenna has radiation pattern with the maximum of radiation in the azimuth plane of the antenna. The radiation characteristics of the end-fire antenna depend on the antenna structure, through which the surface wave propagates, and its magnitude. These types of antennas are Yagi antenna [4], helix antenna with end-fire mode [5], and tapered slot antenna [6].

Today, microstrip antennas have found wide application in the wireless communication field because of their attractive features such as low weight, low profile, small size and easy manufacture. It is fact that microstrip antenna has intrinsically narrow bandwidth [7]. Much research has been done to increase its bandwidth, such as employing a multi-layer structure with aperture coupling [8] and adding parasitic elements [9]. In many practical cases, microstrip antennas are required not only to be wideband but also to have an end-fire radiation pattern. However, most previous researches of microstrip antennas mainly paid attention to the impedance bandwidth of antennas, but ignored the radiation pattern to a certain extent. Very few attempts were made to achieve an end-fire radiation pattern from microstrip antenna.

The antennas having end-fire radiation are widely preferable in many applications for their characteristics such as simplified structure, easy fabrication, cost effectiveness, and low aerodynamic profile. Specially in airborne electronic system, there is a restriction on the antenna orientation as it should not obstruct the airflow during flight. Hence, end-fire antenna is suitable for being used in these applications [10].

Received 22 May 2017, Accepted 13 July 2017, Scheduled 28 July 2017
* Corresponding author: Debajit De (de.debajit118@ieee.org).
The authors are with the Department of Electrical Engineering, National Institute of Technology, Rourkela, India.

This paper focuses on the design of an end-fire unit element microstrip antenna for Traffic Collision Avoidance System (TCAS) of civil aircraft. TCAS is an airborne system which protects its aircraft from mid-air collisions with other aircraft. For surveillance of any surrounding aircraft, TCAS sends interrogation with a consistent rate, ostensibly once every second, and utilizes a recipient for distinguishing the responds to these transmitting signals which are coming from all the transponders of close-by aircraft as shown in Figure 1. For any dangerous situations, TCAS alerts the aircraft pilot by using alarms and displays in the cockpit panel.

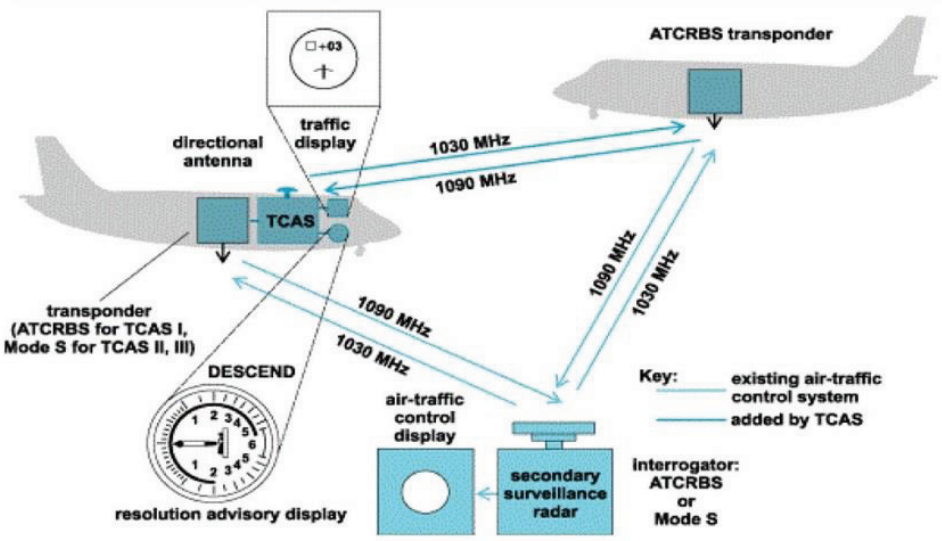

Figure 1. Mid-air surveillance of civil aircraft.

Four classes of TCAS equipment have been identified by the Federal Aviation of Administration (FAA), which are TCAS I, TCAS II, TCAS III and TCAS IV. Out of these versions of TCAS, TCAS II is used in the majority of commercial aviation aircraft. The development of TCAS II has been completed, and the system now enters into the period of operational use. In the existing TCAS II system, four monopole stub elements are used as TCAS directional antenna, and one blade type element is used as TCAS omnidirectional antenna. The TCAS directional antenna is mounted on top of the aircraft, and the TCAS omnidirectional antenna is placed at the bottom of the aircraft. The transmission and reception frequencies of the TCAS antenna are 1.03 GHz and 1.09 GHz, respectively.

The motive of this work is to propose a new antenna technology in TCAS which will have end-fire radiation at both these operating frequencies. Some well-known antennas like Yagi antenna, Vivaldi antenna, half-wavelength slotted antenna and a few more can have end-fire radiation. The basic property of a microstrip antenna is to radiate in the broadside direction. In this paper, an attempt is made to establish the concept that a microstrip antenna with simple modified configuration can also radiate in the end-fire direction just like those conventional end-fired antennas. Again, microstrip antennas are well suited for this application because of their narrow bandwidth characteristics. Moreover, frequency tuning, radiation beam shaping, tuning and steering/scanning are possible in microstrip antenna [11–19]. Microstrip antennas are mechanically very robust, which is one of the significant advantages for using it in this application [20].

Section 2 of this paper explains the design methodology of three proposed antennas, which are Single Patch Single Feed Microstrip Slotted Antenna (SPSFMSA), Dual Patch Single Feed Microstrip Slotted Antenna (DPSFMSA) and Dual Patch Dual Feed Microstrip Slotted Antenna (DPDFMSA). The reason behind this discussion is that step-by-step developments of such an end-fired microstrip antenna have to be shown and discussed in the paper; otherwise, it would have been not possible to establish such a concept. Section 3 deals with the simulation and measurement results of all three proposed antennas. The discussions and summary of these results are also included in this section. The conclusion part of this paper is provided in Section 4.

2. ANTENNA CONFIGURATION AND DESIGN METHODOLOGY

First, a Single Patch Single Feed Microstrip Slotted Antenna is proposed here. After that, a Dual Patch Single Feed Microstrip Slotted Antenna is proposed. Thereafter, using dual feeding technique, the Dual Patch Dual Feed Microstrip Slotted Antenna is designed.

The proposed antennas are designed and simulated in CST Microwave Studio (MWS) and in ANSYS HFSS. Here, Chemical Etching process is used to fabricate all these antennas. FR4 Epoxy is chosen as the substrate material whose dielectric constant (ε_r) is 4.4. Though FR4 Epoxy is a lossy material, it is used here, because this material is easily available in the market and very much cost effective. 1.06 GHz is chosen as the design frequency, since it is center frequency between 1.03 GHz and 1.09 GHz. The dimensions of all these proposed antennas are calculated using the formulae available in the literature [21].

2.1. Single Patch Single Feed Microstrip Slotted Antenna

Figure 2 shows the Single Patch Single Feed Microstrip Slotted Antenna. One single copper patch is designed and used as the radiator. The conventional coaxial feeding technique is used here through which the patch is excited. This copper patch has 4 slots which are abbreviated as Slot 1, Slot 2, Slot 3 and Slot 4. One Shorting Pin/Inductive Post made of copper is put inside the substrate under the patch. The design aspect behind the shorting pin [22] and the slots is fine frequency tuning of the antenna. Shorting pin provides inductance, and slots having length less than $\lambda_0/4$ provide capacitance to the overall antenna. As the frequency goes high, inductive reactance dominates, and as the frequency goes low, capacitive reactance dominates. So, by tuning the diameter of the shorting pin and the length of the slots, proper resonating frequency is achieved here. In this case, shorting pin and slots can be treated as the tuning parameters.

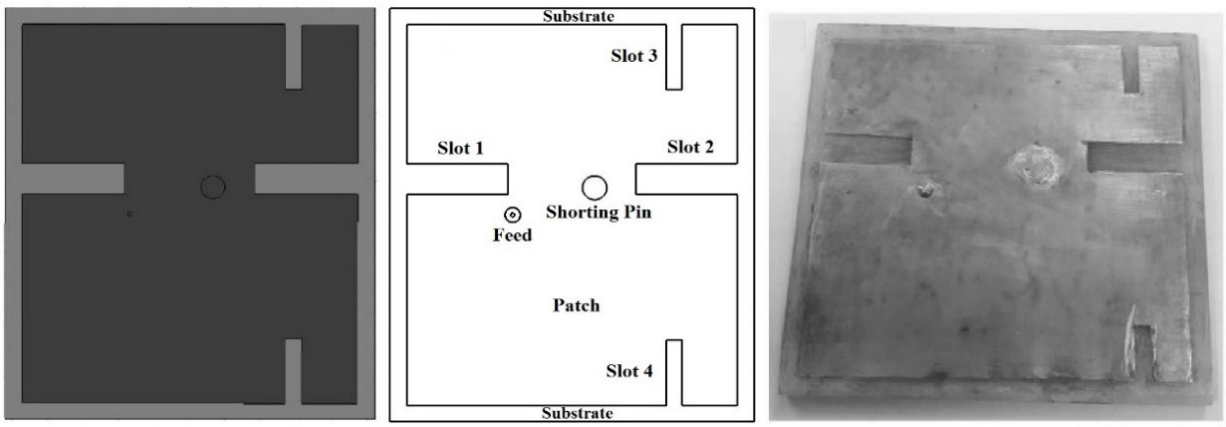

Figure 2. Single patch single feed microstrip slotted antenna: (a) Simulated structure, (b) schematic diagram and (c) fabricated structure.

The dimensions of this proposed antenna are given in Table 1.

In this proposed antenna, the main issue is the radiation pattern. Here, the desired radiation pattern is the end-fire radiation which is along the azimuth plane. However, this proposed antenna provides broadside radiation which is along the elevation plane. Hence, to modify and tune the antenna beam pattern, the concept of a dual-patch antenna is introduced.

2.2. Dual Patch Single Feed Microstrip Slotted Antenna

Figure 3 shows the Dual Patch Single Feed Microstrip Slotted Antenna. This proposed antenna consists of two separate copper patches, which are designed as radiators. The coaxial feeding technique is also

Table 1. Dimensions of the single patch single feed microstrip slotted antenna.

Section	Dimension
Substrate (Length × Width)	104 mm × 121.5 mm
Ground Plane (Length × Width)	104 mm × 121.5 mm
Patch (Length × Width)	95 mm × 112 mm
Slot 1 and Slot 2 (Length × Width)	29 mm × 9 mm
Slot 3 and Slot 4 (Length × Width)	19 mm × 4.5 mm
Diameter of the Shorting Pin	7 mm
Overall Weight	75 grams

used here through which Patch 1 is excited, and by the mutual coupling of electric fields, Patch 2 is also excited. Hence, Patch 1 and Patch 2 are treated as a Primary Radiator and a Secondary Radiator, respectively. One shorting pin made of copper is drilled inside the substrate under Patch 2, and Patch 2 also consists of two narrow slots which are identical but opposite in position to each other. The reasons for using this shorting pin and slots have already been discussed in the previous section.

A triangular shaped metallic cap made of thin copper foil is proposed here, and it is placed above Patch 2 by soldering it with the patch. This metallic cap is separately shown in Figure 4.

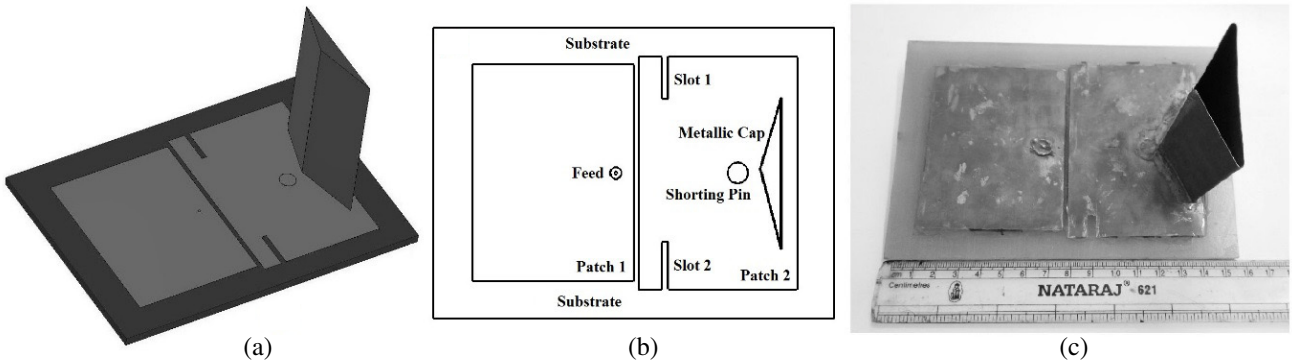

Figure 3. Dual patch single feed microstrip slotted antenna: (a) simulated structure, (b) schematic diagram and (c) fabricated structure.

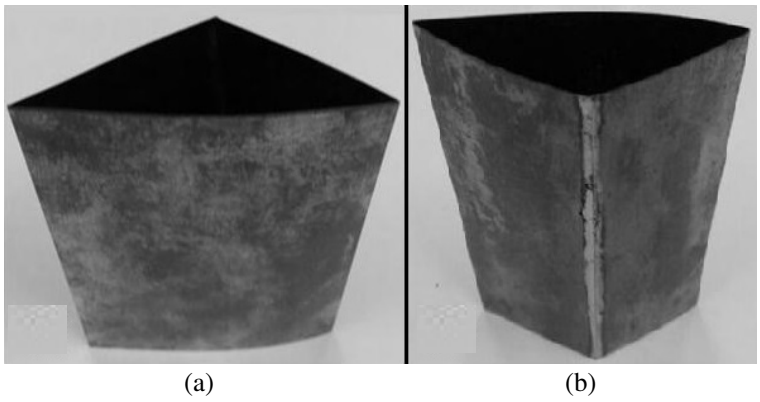

Figure 4. Triangular shaped metallic cap: (a) front view, (b) back view.

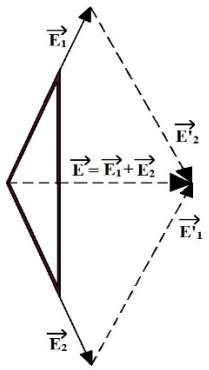

Figure 5. Vector components of electric fields in the metallic cap.

The electric fields in this metallic cap are oriented in such a way that the maximum resultant electric fields can be obtained from the front side of the structure. Figure 5 shows the vector components of the electric fields in the metallic cap. From the figure, it can be seen that the electric field components $\mathbf{E}_1$ and $\mathbf{E}_2$ are radiated from the two adjacent sides of the Metallic Cap. According to the vector addition rule, $\mathbf{E}$ is the resultant vector which can be represented as $\mathbf{E} = \mathbf{E}_1 + \mathbf{E}_2$, and the resultant electric field component $\mathbf{E}$ is radiated from the flatter side (front side) of the metallic cap. Hence, it is expected that the maximum radiation can be achieved from this end. Here, this Metallic Cap is also used to reduce the back radiation so that the antenna can radiate properly along the azimuth plane. The effect of this metallic cap on the back radiation will be shown later.

The dimensions of this proposed antenna are given in Table 2.

Table 2. Dimensions of the dual patch single feed microstrip slotted antenna.

Section	Dimension
Substrate (Length × Width)	157 mm × 110 mm
Ground Plane (Length × Width)	157 mm × 110 mm
Patch 1 (Length × Width)	63.5 mm × 82 mm
Patch 2 (Length × Width)	62.5 mm × 88 mm
Slot 1 and Slot 2 (Length × Width)	16 mm × 2.5 mm
Diameter of the Shorting Pin	8 mm
Height of the Triangular shaped Metallic Cap	65 mm
Gap between Patch 1 and Patch 2	2 mm
Overall Weight	125 grams

In this work, it is proposed that due to the dual-patch radiation and the triangle-shaped metallic cap, microstrip patch antenna can also radiate in the end-fire direction [23].

During the simulation of this antenna, it is observed that at 1.09 GHz, the antenna radiates in the end-fire direction, but at 1.03 GHz, it radiates in the broadside direction. The reason behind this issue is that for 1.09 GHz, the electric fields are in same phase in both the patches, but for 1.03 GHz, the electric fields in Patch 1 are 90° out of phase with the electric fields in Patch 2. This is why it is observed that both the patches can simultaneously radiate at 1.09 GHz. However, at 1.03 GHz, either Patch 1 or Patch 2 radiates due to the 90° phase difference of electric fields between them. Hence, the radiation beam of this proposed single feed antenna can be directed along the azimuth plane at 1.09 GHz but not at 1.03 GHz. To solve this issue, this Dual Patch Dual Feed Microstrip Slotted Antenna is proposed.

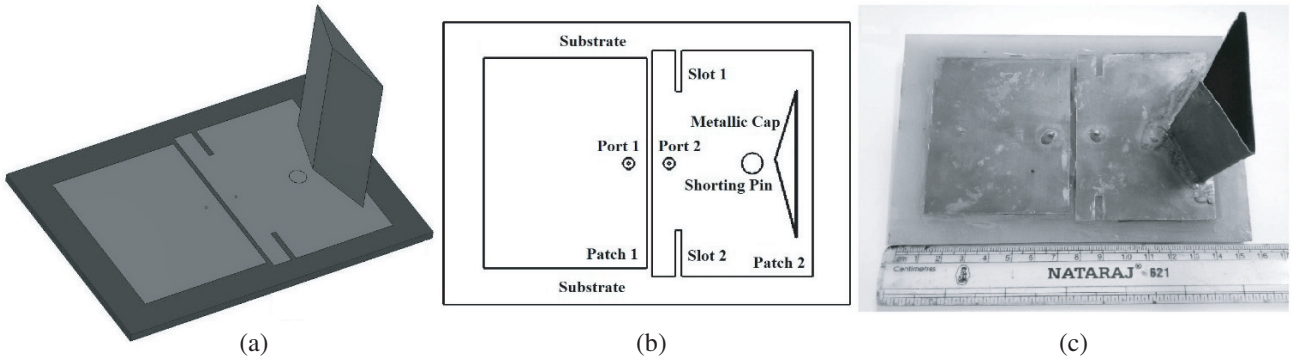

Figure 6. Single patch single feed microstrip slotted antenna: (a) simulated structure, (b) schematic diagram and (c) fabricated structure.

2.3. Dual Patch Dual Feed Microstrip Slotted Antenna

Figure 6 shows the Dual Patch Dual Feed Microstrip Slotted Antenna. This proposed antenna has the same design configuration which is used for the Dual Patch Single Feed Microstrip Slotted Antenna. Here, the only difference is that a separate coaxial feed is applied at Patch 2 to excite it separately. The feeds applied at Patch 1 and Patch 2 are abbreviated as Port 1 and Port 2, respectively. The dimension of this proposed antenna is the same as that of the Dual Patch Single Feed Microstrip Slotted Antenna.

In this antenna, Patch 1 and Patch 2 are excited separately but simultaneously. During the simulation, it is observed that in both the patches, the electric fields are in the same phase for 1.03 GHz and for 1.09 GHz. Hence, this proposed dual-feed antenna can radiate in the end-fire direction for both the operating frequencies.

3. RESULTS AND DISCUSSIONS

All these three proposed antennas are simulated, fabricated and tested for the validation of the design technology. For measurement and testing purpose, Agilent E5071C Vector Network Analyzer (VNA) is used. The radiation patterns of these proposed antennas are measured in a Tapered Anechoic Chamber. During the antenna gain measurement, a double-ridge horn antenna is used as the reference antenna.

3.1. Single Patch Single Feed Microstrip Slotted Antenna

The simulated and measured return losses of the Single Patch Single Feed Microstrip Slotted Antenna are shown in Figure 7. From the simulated results, it is observed that S_{11} is around -32 dB and -27 dB for 1.03 GHz and 1.09 GHz, respectively. The two simulation tools provide similar results. From the measured return loss plot, it is shown that S_{11} is around -26 dB and -20 dB at 1.025 GHz and 1.1 GHz, respectively. Measured return loss is in good agreement with the simulated results, though there are a few disagreements due to measuring environment and fixation of the SMA connectors which are not taken care of during simulation.

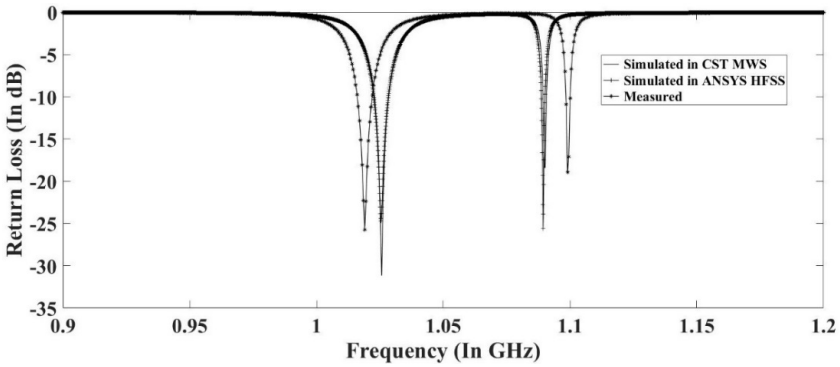

Figure 7. Simulated and measured return loss plot.

Figure 8(a) and Figure 8(b) show the electric field distribution in the patch at 1.03 GHz and 1.09 GHz, respectively. From these plots, it is understood that at 1.03 GHz, the patch has a proper electric field distribution with its dominant mode TM_{010}. However, at 1.09 GHz, the electric field is not properly distributed in the patch. It can be seen that the blue colored electric field zero line splits the whole electric field components at the positions of Slot 1 and Slot 2. The reason behind this behavior is that at 1.09 GHz, the dominant mode TM_{010} is distorted, and an arbitrary mode is generated. The simulated 3D radiation patterns of the antenna for both frequencies are shown in Figure 9. In Figure 9(a), it is observed that at 1.03 GHz, the antenna radiates almost at the broadside direction which is the general feature of a microstrip antenna. However, in Figure 9(b), it can be seen that at 1.09 GHz, the radiating beam is split along the ZX plane due to improper operating mode.

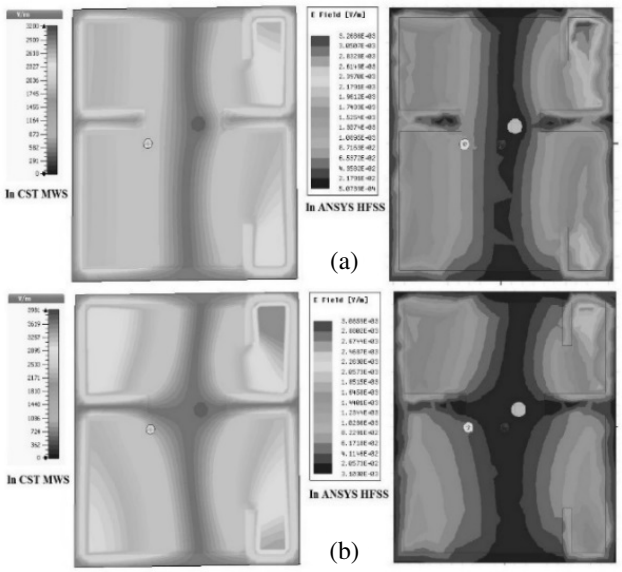

Figure 8. Electric field distribution: (a) at 1.03 GHz and (b) at 1.09 GHz.

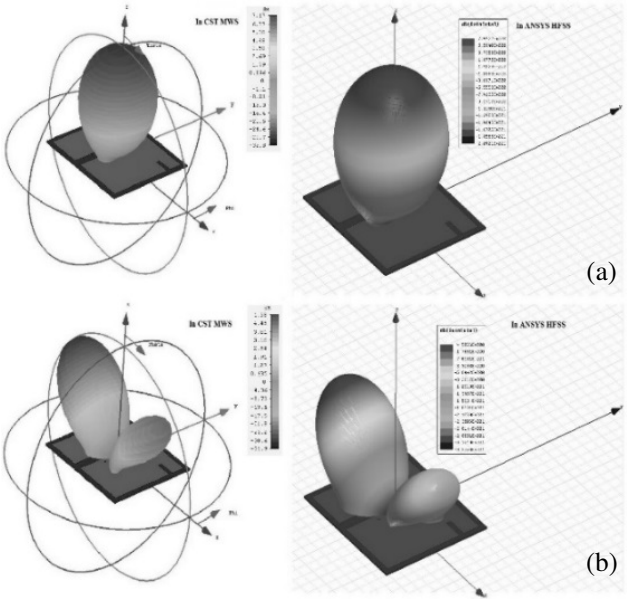

Figure 9. 3D radiation pattern: (a) at 1.03 GHz and (b) at 1.09 GHz.

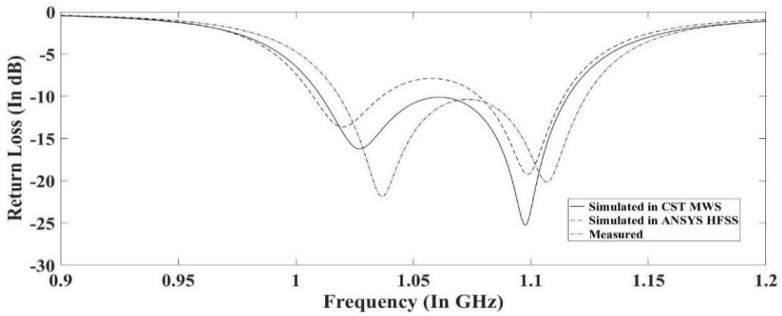

Figure 10. Simulated and measured return loss plot.

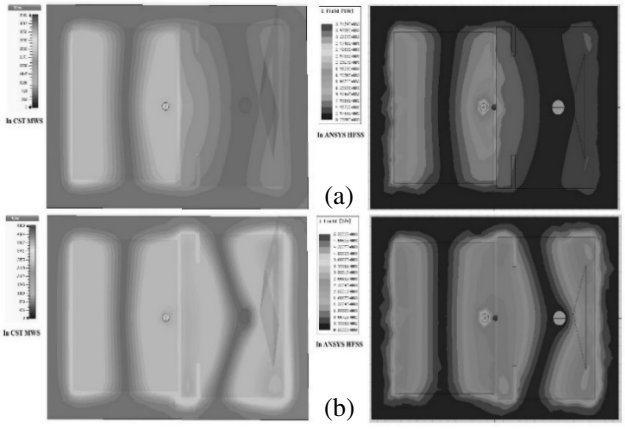

Figure 11. Electric field distribution: (a) at 1.03 GHz and (b) at 1.09 GHz.

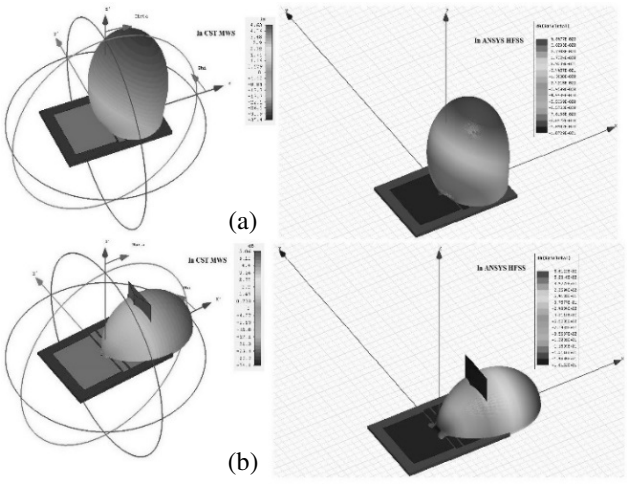

Figure 12. 3D radiation pattern: (a) at 1.03 GHz and (b) at 1.09 GHz.

3.2. Dual Patch Single Feed Microstrip Slotted Antenna

The simulated and measured return losses of the Dual Patch Single Feed Microstrip Slotted Antenna are shown in Figure 10. From the simulated results, it is observed that S_{11} is around -17 dB and -27 dB for 1.03 GHz and 1.095 GHz, respectively. From the measured return loss plot, it is shown that S_{11} is around -23 dB and -22 dB at 1.04 GHz and 1.11 GHz, respectively.

Figure 11(a) and Figure 11(b) show the electric field distribution in the patch at 1.03 GHz and 1.09 GHz, respectively. The simulated 3D radiation pattern of the antenna for both frequencies are shown in Figure 12.

From Figure 11, it can be seen that the proposed antenna has a proper dominant mode TM_{010}. However, the electric field is distributed only in Patch 1 at 1.03 GHz, whereas at 1.09 GHz, both the patches have electric field distribution. This is happened due to the 90° phase lagging issue which has already been described. In Figure 12, it is observed that at 1.03 GHz, the proposed antenna radiates almost at the broadside direction that is along the elevation plane, and at 1.09 GHz, it radiates in the end-fire direction that is along the XY azimuth plane.

3.3. Dual Patch Dual Feed Microstrip Slotted Antenna

The simulated and measured return losses of the Dual Patch Dual Feed Microstrip Slotted Antenna are shown in Figure 13. In this case, the antenna is designed in such a way that Port 1 is responsible for 1.03 GHz, and Port 2 is responsible for 1.09 GHz. From the simulated results, it is observed that S_{11} is around -57 dB at 1.03 GHz, and S_{22} is around -20 dB at 1.095 GHz. From the measured return loss plot, it is shown that S_{11} is around -30 dB at 1.035 GHz, and S_{22} is -18 dB at 1.09 GHz. Here also, the measured return loss is in good agreement with the simulated results.

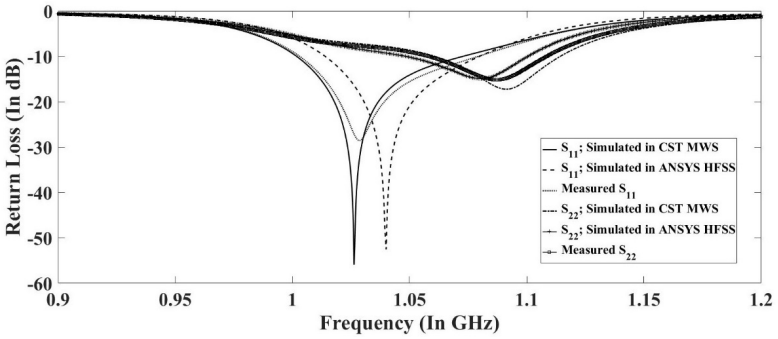

Figure 13. Simulated and measured return loss plot.

For achieving optimized resonating frequency of this proposed antenna and to characterize the antenna design methodology with very fine frequency tuning, various parametric studies are performed. Figure 14(a) shows the variation in return loss, as the width of Slot 1 and Slot 2 is varied from 5 mm to 1 mm. Here, as the width of Slot 1 and Slot 2 is gradually decreased, the capacitive reactance is increased. In general, it is known that the capacitive reactance dominates in the frequency region which is lower than the resonating frequency, and the inductive reactance dominates in the frequency region which is higher than the resonating frequency. Hence in this case, as the capacitive reactance is increased, the resonating frequencies are shifted from high to low.

The variation in return loss is shown in Figure 14(b), when the length of Slot 1 and Slot 2 is varied from 12 mm to 16 mm. Here, as the length of Slot 1 and Slot 2 is gradually increased, the inductive reactance is decreased. As a result, the capacitive reactance is increased. Hence, the 2nd resonating frequency is shifted from high to low.

In Figure 15(a), the variation in return loss is shown as the radius of the shorting pin is varied from 3 mm to 5 mm. Here, as the radius of the shorting pin is gradually increased, the inductive reactance is also increased. Hence in this case, the resonating frequencies are shifted from low to high. Figure 15(b)

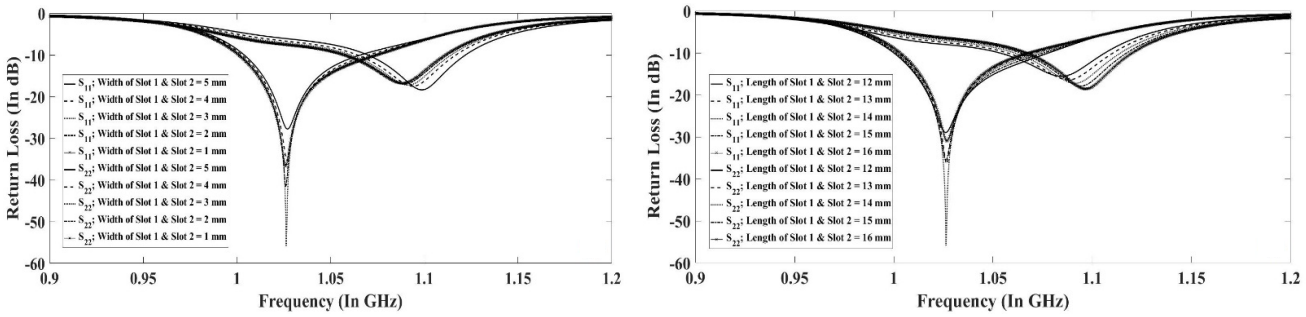

Figure 14. Variation in return loss: (a) by varying width of Slot 1 & Slot 2 and (b) by varying length of Slot 1 & Slot 2.

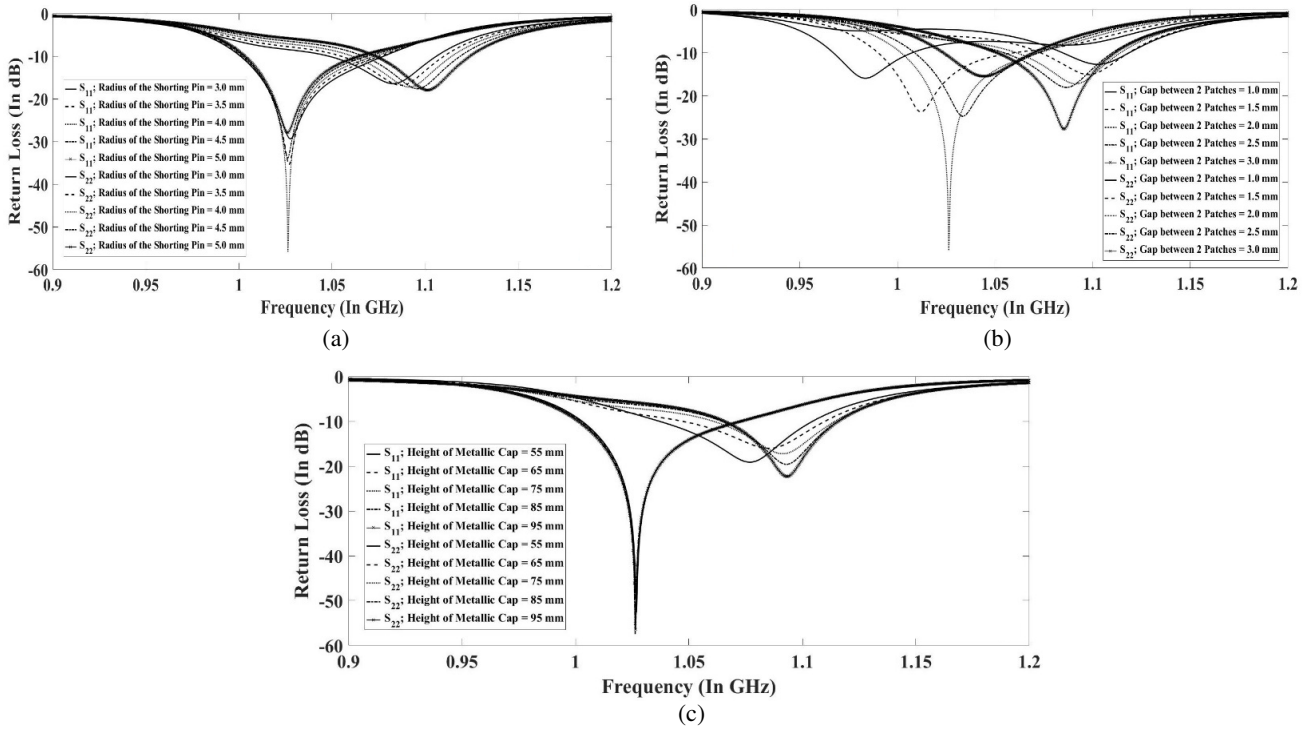

Figure 15. Variation in return loss: (a) by varying the radius of the shorting pin, (b) by varying gap between two patches and (c) by varying height of the metallic cap.

shows the variation in return loss when the gap between the two patches is varied from 1 mm to 3 mm. Similarly, the variation in return loss is shown in Figure 15(c), as the height of the metallic cap is varied from 55 mm to 95 mm.

Figure 16 shows the simulated and measured isolation or coupling between two ports of the antenna. From Figure 16, it is observed that S_{12} is around -5 dB at both the operating frequencies. As S_{12} is close to 0 dB, it is understood that the two ports are well coupled, as it is expected when the orientations of the two patches are 180° to each other with regard to the feed locations. The variation in isolation is shown in Figure 17, as the gap between the two patches is varied from 0.5 mm to 8.5 mm. It is observed that as the gap between the two patches is gradually increased from 0.5 mm to 8.5 mm, the coupling between Port 1 and Port 2 is subsequently reduced.

Figure 18(a) and Figure 18(b) show the electric field distribution in the patch at 1.03 GHz and 1.09 GHz, respectively. From these plots, it is understood that the proposed antenna has the proper

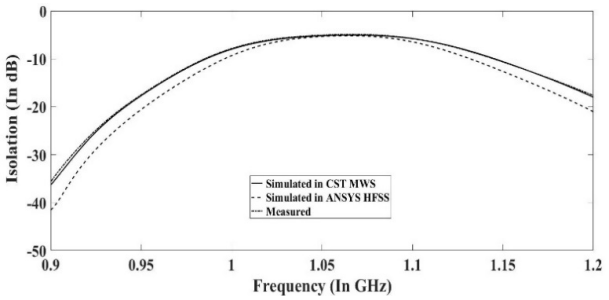

Figure 16. Simulated and measured isolation between Port 1 and Port 2.

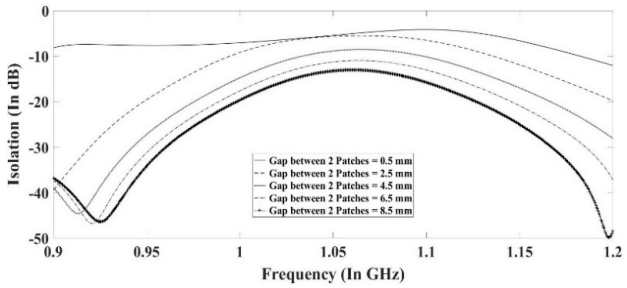

Figure 17. Variation in isolation by varying by varying gap between two patches.

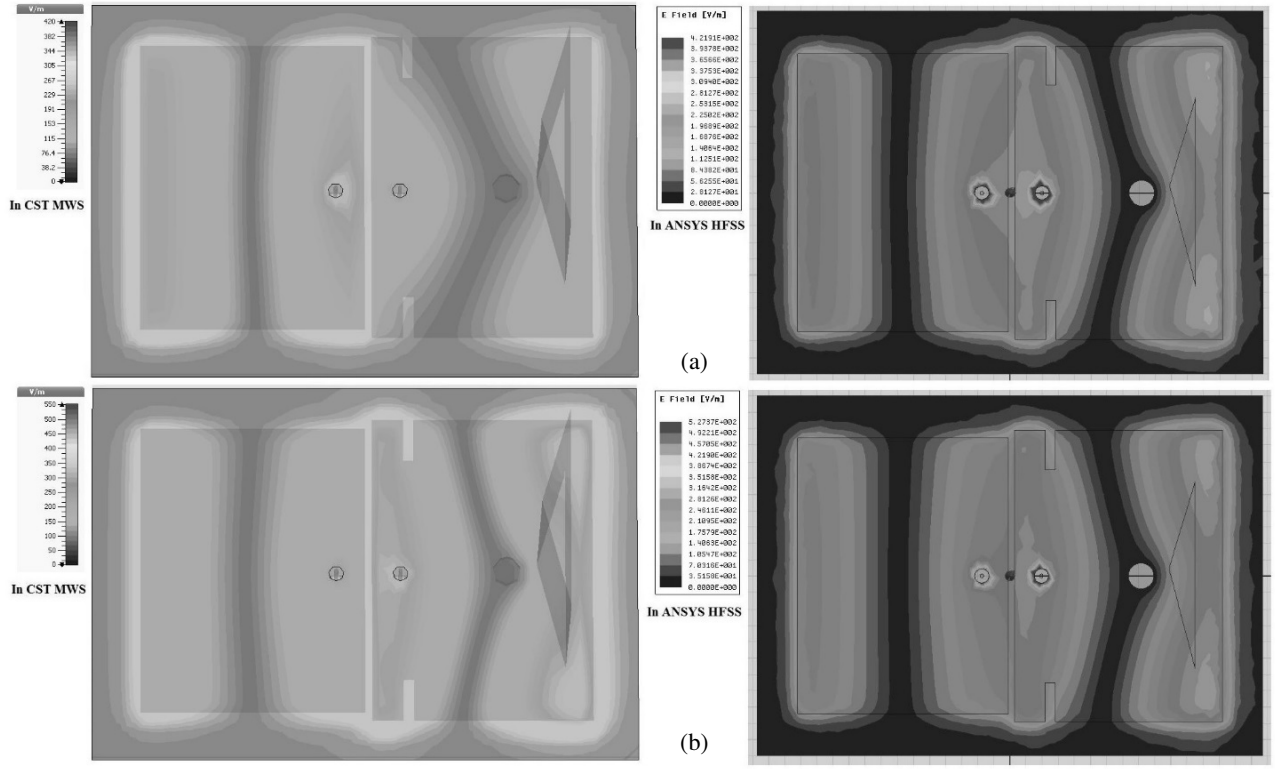

Figure 18. Electric field distribution: (a) at 1.03 GHz and (b) at 1.09 GHz.

dominant mode TM_{010}. The electric fields are in the same phase in both the patches for 1.03 GHz and 1.09 GHz. Hence, both the patches have almost equal electric field distribution at these two operating frequencies. It is seen that the electrical path lengths between the electric-field-zero lines corresponding to the blue colored ones in the two patches are almost the same for these two frequencies. Hence, it explains that the tow patches together will radiate in such a way that the power patterns at two said frequencies will be nearly same. As the electric-field-zero lines remain same at both the frequencies, these can be considered as reference lines for measurement of the feed point path length in terms of standing wave pattern in each patch.

The simulated 3D radiation patterns of the antenna for both frequencies are shown in Figure 19. In Figure 19, it is observed that at 1.03 GHz and 1.09 GHz, the antenna radiates in the end-fire direction that is along the XY azimuth plane. As the coupling between Port 1 and Port 2 is maintained at such a high level, the electrical path lengths between the electric-field-zero lines in the two patches are almost the same for both the operating frequencies. Hence, the resultant radiated electric fields of Patch 1 and

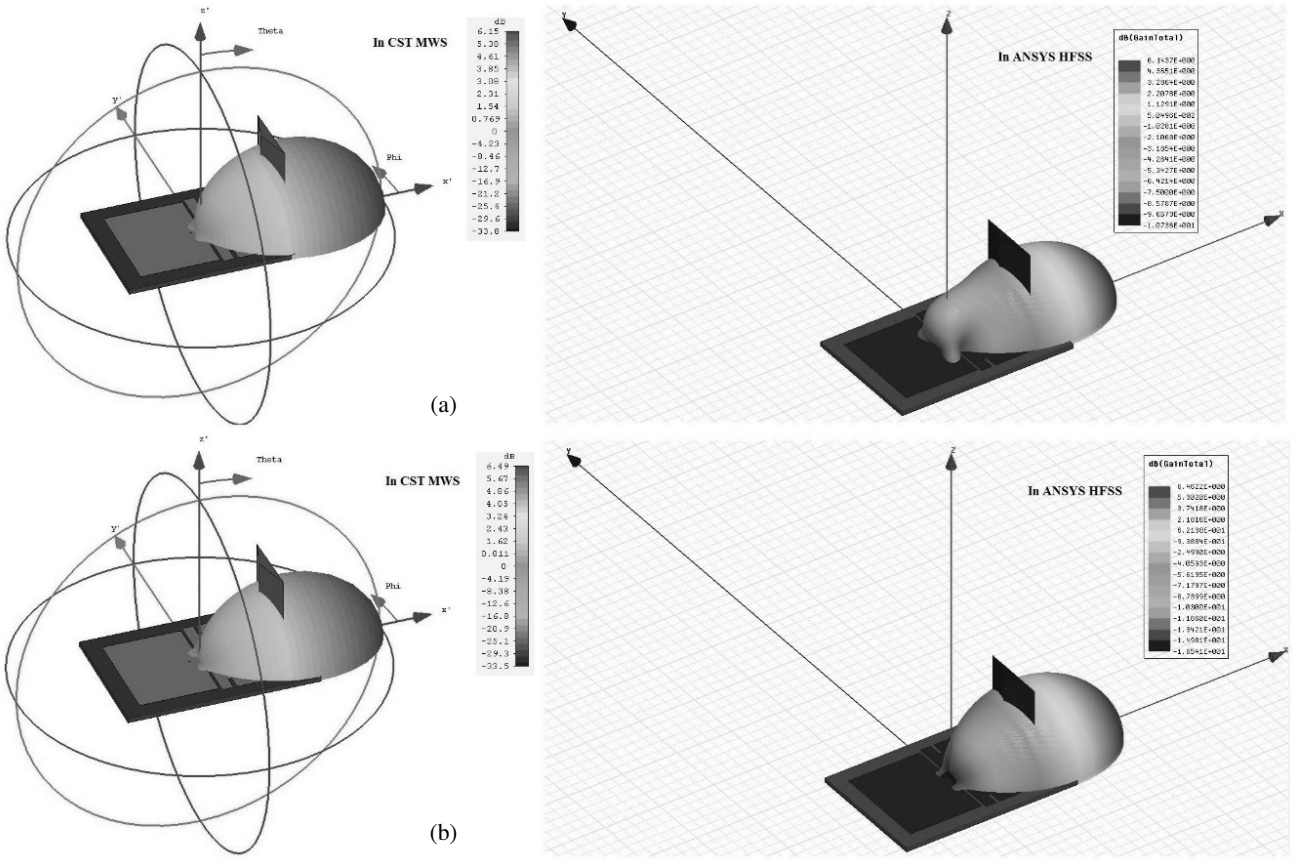

Figure 19. 3D radiation pattern: (a) at 1.03 GHz and (b) at 1.09 GHz.

Patch 2 are directed towards the end-fire direction.

It is investigated that if the coupling between Port 1 and Port 2 is very little, the electrical path lengths between the electric-field-zero lines in two patches will not remain same for 1.03 GHz and 1.09 GHz. This is because of the issue related to the phase difference of electric fields in the patches which was reported in the case of Dual Patch Single Feed Antenna. Hence, in that scenario, the antenna cannot radiate similarly and properly in the end-fire direction for those two frequencies.

The effect on end-fire radiation by varying the height of the metallic cap is shown in Figure 20. From this figure, it is observed that as the height of the metallic cap is increased from 25 mm to 65 mm, the back radiation is gradually reduced, and finally it is diminished when the height of the metallic cap is 65 mm.

A CAD Model of Boeing-787 Aircraft is designed here. During the simulation setup, first the proposed antenna is mounted on the top of the aircraft, and then, it is simulated with the aircraft model. The corresponding 3D radiation patterns are shown in Figure 21. The purpose of this study is to observe the Antenna Installed Performance on a large electrical structure. To simulate this large aircraft structure, the asymptotic solver is used instead of FIT (finite integration technique) solver, because this numerical technique can simulate large problems with available hardware resources by using acceleration techniques like multi-core/CPU computing or distributed computing. Also, the separation of complex problems into multiple parts and with the link between them being defined by equivalent near or far field sources, this technique can dramatically speed up the analysis of antenna installed performance. From the results, it is observed that the beam pattern has not been distorted due to this large electrical structure.

The simulated and measured power patterns of the antenna in XY elevation plane and ZX elevation plane for 1.03 GHz are shown in Figure 22(a) and Figure 22(b), respectively. Similarly, Figure 23(a)

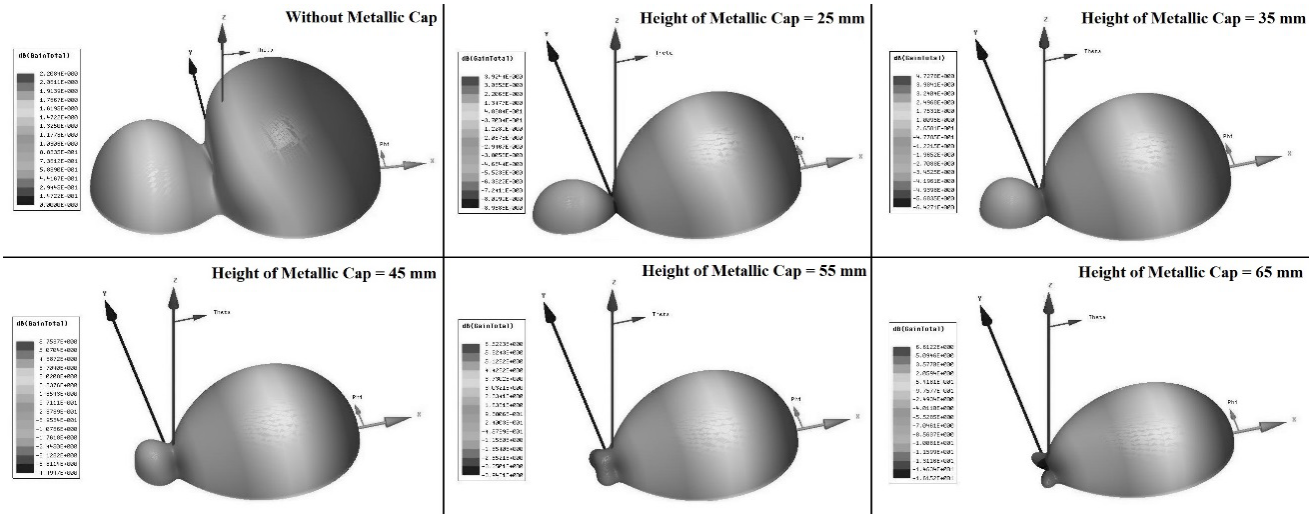

Figure 20. Effect on end-fire radiation pattern due to various height of the metallic cap.

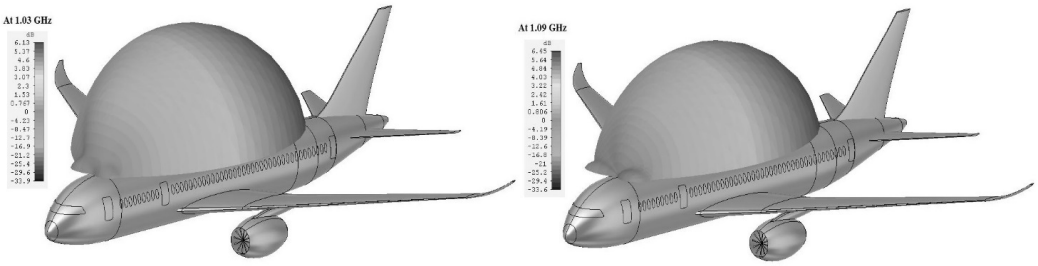

Figure 21. Antenna installed performance at 1.03 GHz and at 1.09 GHz.

and Figure 23(b) show the power patterns of the antenna for 1.09 GHz. The whole body of the aircraft is itself a ground plane. Hence during the power pattern and antenna gain measurement, the proposed antenna is placed over a large metallic ground plane of size 10 m × 10 m for realizing the presence of the aircraft body upto some extent. From Figure 22(a) and Figure 23(a), it is observed that the antenna radiates maximum at around 0° of the XY azimuth plane which shows that this antenna provides end-fire radiation at 1.03 GHz and 1.09 GHz. Here, co-polarization level is around −10 dBW, and the cross-polarization level is well below −50 dBW. Hence, the co-pol is almost not affected by the cross-pol. In Figure 22(b) and Figure 23(b), it can also be seen that the maximum co-pol of the relative power is achieved at around +90° in the ZX elevation plane for both the operating frequencies, and subsequently it also proves that the maximum radiation from the antenna is towards the end-fire direction.

Figure 24 shows the simulated and measured peak gains of the proposed antenna at $\varphi = 0°$ in XY plane. It is shown that at $\varphi = 0°$ in XY plane, the simulated antenna gain is around 6.2 dB at 1.03 GHz and around 6.5 dB at 1.09 GHz. The measured antenna gain is around 5.5 dB at 1.03 GHz and around 6.7 dB at 1.09 GHz. Figure 25 shows the simulated and measured axial ratios of the proposed antenna at $\varphi = 0°$ in XY plane. It is shown that at $\varphi = 0°$ in XY plane, the simulated axial ratio is around 327 dB at 1.03 GHz and around 325 dB at 1.09 GHz. The measured axial ratio is around 321 dB at 1.03 GHz and around 324 dB at 1.09 GHz. Here, all the values of the axial ratio are sufficiently more than 0 dB at both the operating frequencies. Hence, it is understood that this antenna is linearly polarized.

The simulated and measured radiation efficiencies of the proposed antenna are shown in Figure 26. It is understood that the simulated radiation efficiency is around 54% at 1.03 GHz and around 47% at 1.09 GHz, while the measured radiation efficiency is around 46% at 1.03 GHz and around 53% at 1.09 GHz.

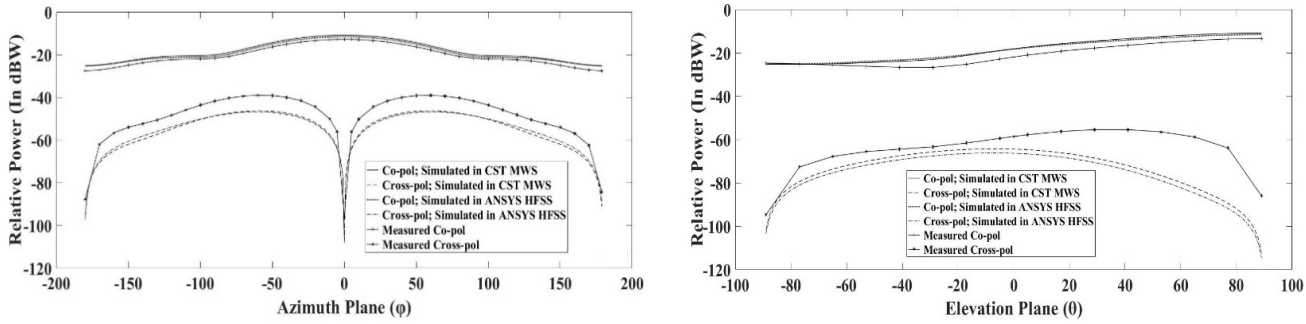

Figure 22. Simulated and measured power pattern plot for 1.03 GHz: (a) in XY plane and (b) in ZX plane.

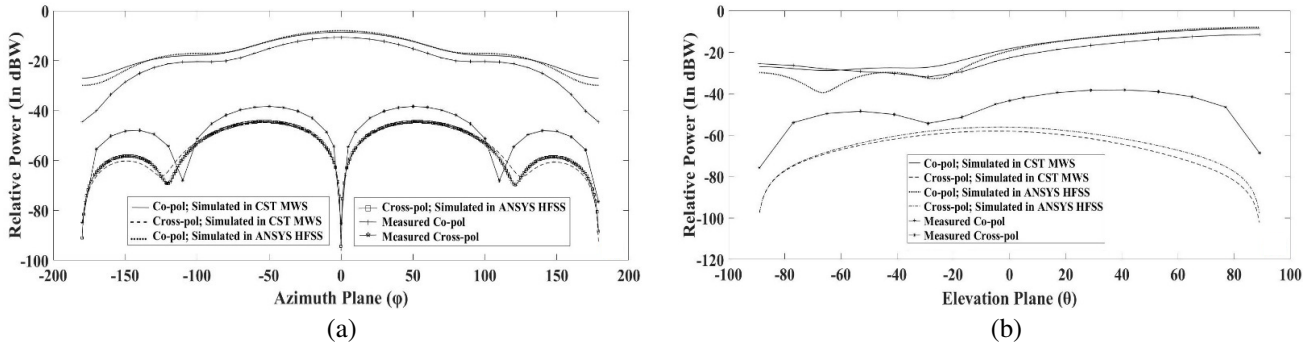

Figure 23. Simulated and measured power pattern plot for 1.09 GHz: (a) in XY plane and (b) in ZX plane.

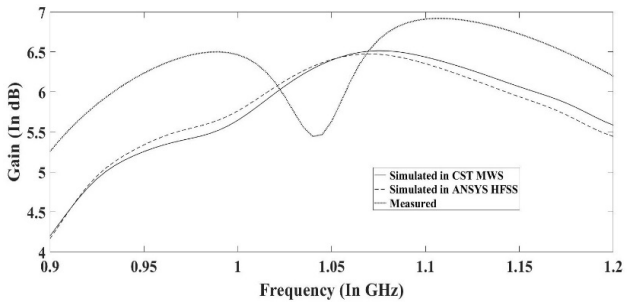

Figure 24. Simulated and measured antenna gain vs. frequency plot at $\varphi = 0°$ in XY plane.

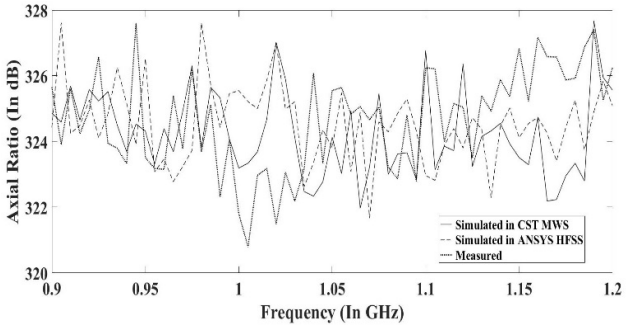

Figure 25. Simulated and measured axial ratio vs. frequency plot at $\varphi = 0°$ in XY plane.

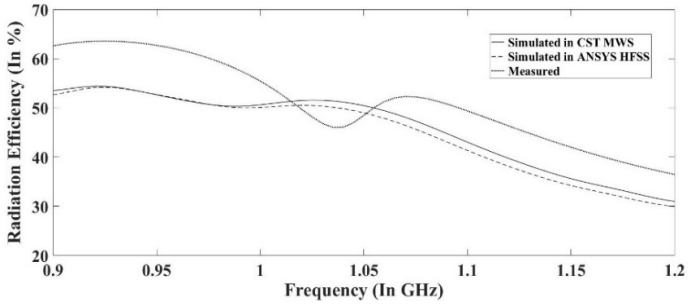

Figure 26. Simulated and measured antenna radiation efficiency vs. frequency plot.

3.4. Summary and Performance Comparison between the Proposed Antennas

Table 3 summarizes all the simulation and measurement results of these three proposed antennas. This table also helps to observe the performance comparison between these antennas.

The proposed Dual Patch Dual Feed Microstrip Slotted Antenna is the optimized model, and hence it provides the best results in terms of frequency sensitivity, desired end-fire radiation pattern,

Table 3. Performance comparison between the proposed antennas.

Parameters				SPSFMSA	DPSFMSA	DPDFMSA
Operating Frequencies (In GHz)	f_1	Simulated	In CST	1.03	1.03	1.03
			In HFSS	1.03	1.025	1.04
		Measured		1.025	1.04	1.035
	f_2	Simulated	In CST	1.09	1.095	1.095
			In HFSS	1.09	1.095	1.085
		Measured		1.1	1.11	1.09
Return Loss (In dB)	at f_1	Simulated	In CST	-32	-17	-57
			In HFSS	-25	-14	-54
		Measured		-26	-23	-30
	at f_2	Simulated	In CST	-20	-27	-15
			In HFSS	-27	-20	-15
		Measured		-20	-22	-18
Gain (In dB)	at f_1	Simulated	In CST	7.2	4.6	6.2
			In HFSS	7.5	4.8	6.1
		Measured		7.6	3.8	5.5
	at f_2	Simulated	In CST	4.5	5.1	6.5
			In HFSS	4.5	5.6	6.5
		Measured		5	5	6.7
Beamwidth (In degree)	at f_1	Simulated	In CST	86	82	79
			In HFSS	88	80	78
		Measured		94	89	84
	at f_2	Simulated	In CST	-	81	77
			In HFSS	-	80	76
		Measured		-	85	81
Side Lobe (In dB)	at f_1	Simulated	In CST	-19.9	-13.3	-15.7
			In HFSS	-19.7	-12.9	-15.5
		Measured		-17.9	-17.9	-10.4
	at f_2	Simulated	In CST	-	-11.8	-12
			In HFSS	-	-11.5	-12.1
		Measured		-	-	-9.5
Axial Ratio (In dB)	at f_1	Simulated	In CST	50	60	327
			In HFSS	50	42	327
		Measured		40	40	55
	at f_2	Simulated	In CST	30	327	323
			In HFSS	20	327	325
		Measured		23	23	325
Radiation Efficiency (In %)	at f_1	Simulated	In CST	88	62	54
			In HFSS	86	50	52
		Measured		87	87	53
	at f_2	Simulated	In CST	52	52	47
			In HFSS	48	50	45
		Measured		55	55	45
Radiation Pattern	at f_1	Simulated	In CST	Directional & Broadside	Directional & Broadside	Directional & End-Fire
			In HFSS	Directional & Broadside	Directional & Broadside	Directional & End-Fire
		Measured		Directional & Broadside	Directional & Broadside	Directional & Broadside
	at f_2	Simulated	In CST	Directional & Distorted	Directional & End-Fire	Directional & End-Fire
			In HFSS	Directional & Distorted	Directional & End-Fire	Directional & End-Fire
		Measured		Directional & Distorted	Directional & End-Fire	Directional & End-Fire

gain, beamwidth and side-lobe level. From Table 3, it is observed that the beamwidth of this proposed antenna is reduced as compared to that of other two antennas. Due to this narrow beamwidth, resolving the location of the intruder aircraft in terms of bearing angle is much better, and hence the resolution power of this proposed antenna is better than the others. As shown in Table 3, the side lobe level of this proposed antenna is around -15 dB. Hence, the sensitivity of the proposed antenna is expected to be better. Due to this low level of side lobe in this proposed antenna and if this low level is considered to be the threshold value of return signal, the covering distance will likely to become more. As the covering distance is larger, larger number of aircraft, which are hither to unseen in the existing system, can be detected. So, larger number of aircraft can be tracked for collision probability with respect to the own aircraft.

4. CONCLUSION

This paper presents a designing technique for microstrip antenna which has end-fire radiation, and hence it can be used in many airborne systems like TCAS and Transponder. From Table 2, it is understood that the proposed Dual Patch Dual Feed Microstrip Slotted Antenna is very compact in size and weights around 125 grams. Hence, this new proposed antenna is also very light in weight as compared to that of existing TCAS II antenna whose weight is around 800 grams. This proposed antenna is also cost effective since FR4 epoxy substrate is used here. The width and length of the patch are determined for conforming to the space section accessible for the overall fuselage area in the aircraft. The ongoing research focus is on the development of a compact microstrip end-fire array where this proposed unit element will be used as the array element, and it will be designed in such a way that the whole antenna structure can effectively cover the forward and rear directions with high front-to-back ratio. This proposed antenna will be fitted on the top fuselage of the aircraft, and it will not be left open. It will be encapsulated inside an aerodynamically shaped enclosure, known as Radome. For a high speed carrier, a radome of low profile must be used to reduce the air drag. Research on the designing of such shaped encapsulation for this proposed antenna is still going on.

Therefore, the proposed Dual Patch Dual Feed Microstrip Slotted antenna will be expected to meet the requirements of the advanced avionics standards in terms of design simplicity, lightweight and high performance.

REFERENCES

1. Ammann, M. J. and Z. N. Chen, "Wideband monopole antennas for multi-band wireless systems," *IEEE Antennas and Propagation Magazine*, Vol. 45, No. 2, 146–150, 2003.
2. Booker, H. G., "Slot aerials and their relation to complementary wire aerials (Babinet's principle)," *Journal of the Institution of Electrical Engineers — Part IIIA: Radiolocation*, Vol. 93, No. 4, 620–626, 1946.
3. Wong, K. L. and W. H. Hsu, "A broad-band rectangular patch antenna with a pair of wide slits," *IEEE Transactions on Antennas and Propagation*, Vol. 49, No. 9, 1345–1347, 2001.
4. DeJean, G. R., T. T. Thai, S. Nikolaou, and M. M. Tentzeris, "Design and analysis of microstrip Bi-Yagi and Quad-Yagi antenna arrays for WLAN applications," *IEEE Antennas and Wireless Propagation Letters*, Vol. 6, 244–248, 2007.
5. Ehrenspeck, H., "The double-helix antenna and its variants, a new class of tunable endfire antennas," *IEEE Transactions on Antennas and Propagation*, Vol. 13, No. 2, 203–208, 1965.
6. Pazin, L. and Y. Leviatan, "A compact 60-GHz tapered slot antenna printed on LCP substrate for WPAN applications," *IEEE Antennas and Wireless Propagation Letters*, Vol. 9, 272–275, 2010.
7. Kraus, J. D. and R. J. Marhefka, *Antennas: For All Applications*, 3rd Edition, The McGraw-Hill Companies Inc., 2002.
8. Targonski, S. D., R. B. Waterhouse, and D. M. Pozar, "Design of wide-band aperture-stacked patch microstrip antennas," *IEEE Transactions on Antennas and Propagation*, Vol. 46, No. 9, 1245–1251, 1998.

9. Abdelaziz, A. A., "Bandwidth enhancement of microstrip antenna," *Progress In Electromagnetics Research*, Vol. 63, 311–317, 2006.
10. Sanyal, A., A. Basu, S. K. Koul, M. Abegaonkar, S. Varughese, and P. B. Venkatesh Rao, "A planar end-fire array in S-band for airborne applications," *IETE Journal of Research*, Vol. 58, No. 1, 34–43, 2014.
11. Saed, M. A., "Broadband CPW-fed planar slot antennas with various tuning stubs," *Progress In Electromagnetics Research*, Vol. 66, 199–212, 2006.
12. Eldek, A. A., A. Z. Elsherbeni, and C. E. Smith, "Dual-wideband square slot antenna with a U-shaped printed tuning stub for personal wireless communication systems," *Progress In Electromagnetics Research*, Vol. 53, 319–333, 2005.
13. Eldek, A. A., A. Z. Elsherbeni, and C. E. Smith., "Design of wideband triangle slot antennas with tuning stub," *Progress In Electromagnetics Research*, Vol. 48, 233–248, 2004.
14. Kale, G. M., R. P. Labade, and R. S. Pawase, "Tunable and dual band rectangular microstrip antenna for bluetooth and WiMAX applications," *Microwave and Optical Technology Letters*, Vol. 57, No. 8, 1986–1991, 2015.
15. Tsai, J. F., C. J. Shih, and J. S. Row, "A design method for patch antennas with wide frequency tunable range and stable conical radiation," *Microwave and Optical Technology Letters*, Vol. 54, No. 6, 1441–1445, 2012.
16. Attia, H., O. Siddiqui, and O. Ramahi, "Beam tilting of single microstrip antenna using high permittivity superstrate," *Microwave and Optical Technology Letters*, Vol. 55, No. 7, 1657–1661, 2013.
17. Binoy, G. S., C. K. Aanandan, P. Mohanan, and K. Vasudevan, "Dual-frequency dual-polarized slot-coupled compact microstrip antenna for communication systems," *International Journal of Electronics*, Vol. 89, No. 3, 191–195, 2010.
18. Jayasinghe, J. M. J. W., J. Anguera, D. N. Uduwawala, and A. Andújar, "High-directivity genetic microstrip patch antenna," *International Journal of Electronics Letters*, Vol. 4, No. 3, 279–286, 2015.
19. Wu, W., B. Z. Wang, and S. Sun, "Pattern reconfigurable microstrip patch antenna," *Journal of Electromagnetic Waves and Applications*, Vol. 19, No. 1, 107–113, 2012.
20. Orban, D. and G. J. K. Moernaut, "The basics of patch antennas," *RF Globalnet Newsletter*, 2009.
21. Balanies, C. A., *Antenna Theory: Analysis & Design*, 2nd Edition, John Wiley & Sons Inc., 1997.
22. Singh, A. K. and M. K. Meshram, "Shorting pin loaded dual-band compact rectangular microstrip antenna," *International Journal of Electronics*, Vol. 94, No. 3, 237–250, 2007.
23. Chen, K., X. Chen, and K. Huang, "A novel microstrip dipole antenna with wideband and end-fire properties," *Journal of Electromagnetic Waves and Applications*, Vol. 21, No. 12, 1679–1688, 2012.